AD_____

Award Number: W81XWH-12-1-0286

TITLE:
Improving the Diagnostic Specificity of CT for Early Detection of Lung Cancer: 4D CT-Based Pulmonary Nodule Elastometry

PRINCIPAL INVESTIGATOR:
Peter G Maxim, PhD

CONTRACTING ORGANIZATION:
The Leland Stanford Junior University

Stanford, CA 94305-2004

REPORT DATE:
August 2014

TYPE OF REPORT:
Annual

PREPARED FOR: U.S. Army Medical Research and Materiel Command
Fort Detrick, Maryland 21702-5012

REPORT DOCUMENTATION PAGE

Form Approved
OMB No. 0704-0188

1. REPORT DATE	2. REPORT TYPE	3. DATES COVERED
August 2014	Annual	15 Jul 2013 - 14 Jul 2014

4. TITLE AND SUBTITLE

Improving the Diagnostic Specificity of CT for Early Detection of Lung Cancer: 4D CT-Based Pulmonary Nodule Elastometry

5a. CONTRACT NUMBER

5b. GRANT NUMBER
W81XWH-12-1-0286

5c. PROGRAM ELEMENT NUMBER

6. AUTHOR(S)

Peter G Maxim, PhD,
Billy W Loo, MD, PhD

E-Mail: pmaxim@stanford.edu

5d. PROJECT NUMBER

5e. TASK NUMBER

5f. WORK UNIT NUMBER

7. PERFORMING ORGANIZATION NAME(S) AND ADDRESS(ES)

THE LELAND STANFORD JUNIOR UNIVERSITY
450 SERRA MALL
STANFORD, CA 94305-2004

8. PERFORMING ORGANIZATION REPORT NUMBER

9. SPONSORING / MONITORING AGENCY NAME(S) AND ADDRESS(ES)
U.S. Army Medical Research and Materiel Command
Fort Detrick, Maryland 21702-5012

10. SPONSOR/MONITOR'S ACRONYM(S)

11. SPONSOR/MONITOR'S REPORT NUMBER(S)

12. DISTRIBUTION / AVAILABILITY STATEMENT
Approved for Public Release; Distribution Unlimited

13. SUPPLEMENTARY NOTES

14. ABSTRACT

In this study we propose to develop and validate pulmonary nodule elastometry imaging, a method complementary to CT that has the potential to increase the specificity of screening for early detection of lung cancer. We propose to address the need for greater specificity in lung cancer screening by characterizing a mechanical property of pulmonary lesions, specifically pulmonary nodule (PN) elasticity, in addition to standard anatomic features. We hypothesize that malignant and benign PN can be distinguished more specifically by different elasticities determined from 4D CT images. The specific aims of the study were the development of pulmonary nodule elastometry algorithms based on deformable image processing of 4D CT images and their validation in an animal model and in a retrospective review of over 200 4D CT scans from patients with small malignant pulmonary nodules previously treated with radiation in our department. We have successfully developed the algorithms, and in a first validation we have demonstrated proof of principles that elastometry can distinguish malignant PNs from surrounding lung tissue (a manuscript is in preparation. The validation in animal models and the retrospective analysis of the human data is ongoing.

15. SUBJECT TERMS
Pulmonary nodule elastometry, 4DCT, deformable image registration, Jacobian, lung cancer, lung cancer screening

16. SECURITY CLASSIFICATION OF:			17. LIMITATION OF ABSTRACT	18. NUMBER OF PAGES	19a. NAME OF RESPONSIBLE PERSON
a. REPORT	b. ABSTRACT	c. THIS PAGE			USAMRMC
U	U	U	UU	28	19b. TELEPHONE NUMBER *(include area code)*

Table of Contents

Page

Contract number: W81XWH-12-1-0286

Title: Improving the Diagnostic Specificity of CT for Early Detection of Lung Cancer: 4D CT-Based Pulmonary Nodule Elastometry

Principal Investigator: Peter G Maxim, PhD

Introduction:

In this project we are addressing a shortcoming of existing lung cancer screening methods by developing a CT based method of characterizing a mechanical property of pulmonary lesions, specifically tissue elasticity (stiffness) that should have a higher specificity than purely anatomic low-dose CT. It is the aim of the proposed study to decrease the false positive rate of CT screening by analyzing the mechanical properties of suspiciously appearing tissue during CT screening. We hypothesize that malignant pulmonary nodules are less elastic (stiffer) than benign nodules and that this difference in elasticity can be used to differentiate cancerous from benign nodules, which would help to decrease the false positive rates of CT screening. A measure of elasticity can be derived from high-resolution 4-dimensional computed tomography (4D CT) using deformable image registration algorithms. Unlike conventional 3D CT imaging that results in a static image of the scanned anatomy, 4D CT incorporates also the temporal changes of the anatomy caused by respiratory motion, yielding a CT 'movie' that allows the evaluation of tumor motion and the calculation of the elasticity.

Body:

Specific Aim 1. Development of deformable image algorithms for processing the 4D CT images to determine the elasticity of malignant and benign pulmonary nodules. *(**Dr. Maxim**, Tasks 1, months 1 – 8)*

Task 1. Development of the software for deformable image registration, analysis of the DVF and the calculation of the elasticity parameter (Matlab).

*The software will be developed using the mathematical package Matlab (The Mathworks Inc., Natick, MA). Two deformable image registration algorithms will be used (DIR^{vol} and a method based on optical flow, DIR^{OF}). The resulting displacement vector fields will be analyzed and an elasticity parameter for the pulmonary nodules will be calculated (**Dr. Maxim**, months 1 – 8).*

Status (Task 1):

A manuscript describing our algorithm and its validation has been submitted to 'Radiotherapy and Oncology' (Green Journal) and is attached to this report.

Specific Aim 2: Validate our method in rat models of human lung cancer and benign inflammatory lesions. *(**Dr. Maxim**, Tasks 2-4, months 3 – 24)*

Task 2. ***Preliminary experiments: Establish optimal protocol for the benign pulmonary model (granulomatous inflammation) and study growth kinetics.***

*2a. Purchase animals: Rowett rats, A549 and SK-MES-1 cells from American Tissue Culture Collection (ATCC), carbon nanotubes (catalogue number 900–1501, lot GS1801), SES research (Houston, TX) and necessary culturing media. (**Dr. Maxim**, months 1-3)*

*2b. Inoculate 15rats (Rowett nude rats) with carbon nanotubes and follow with serial MicroCT measurements to study growth kinetics to establish the time for nodule development to reach desired size. (**Dr. Maxim**, 15 rats total, months 3 – 6)*

Task 3. ***Grow orthotopic model of lung cancer and benign lesions and follow with serial MicroCT imaging: preliminary experiments to establish protocol and optimize software***

*3a. Inoculate 10 rats with orthotopic human lung cancer cells (A549, left lung) and carbon nanotubes (right lung) (**Dr. Maxim**, months 7-9)*

*3b. Acquire CT images at peak-inhale and peak-exhale using a small animal ventilator (**Dr. Maxim**, month 9-10)*

*3c. Analyze CT images and derive elasticity parameter and optimize software if necessary. (**Dr. Maxim**, month 10)*

Task 4. ***Grow orthotopic model of lung cancer and benign lesions and follow with serial MicroCT imaging, analyze data***

*4a. Inoculate remaining 40 rats (A549 cells, left lung in Rowett nude rats) and follow with CT imaging at peak-inhale and peak-exhale (**Dr. Maxim**, months11-13)*

*4b. Perform simplified analysis: Delineate malignant and benign pulmonary nodules and measure volumes at peak-inhale and peak-exhale. Derive elasticity parameter based on the ratio of the volumes. (**Dr. Maxim**, months 14-15)*

*4c. Analyze acquired CT images and derive elasticity parameter by analyzing the displacement vector fields and perform statistical analysis. (**Dr. Maxim**, months 16-18)*

*4d. Repeat experiments and analysis with second cancer cell line (SK-MES-1), 50 Rowett rats, (**Dr. Maxim**, months 18-23)*

*4e. Publish animal study results (**Dr. Maxim**, month 24)*

Status (Tasks 2, 3, 4): Due to ongoing repairs and upgrades of the GE-MicroCT scanner, our proposed experiments are being delayed again. The capability of acquiring 4DCT images is hampered by a defect in the GE-MicroCT scanner. Given this delay, we asked the DoD for a one-year no-cost extension, which was recently approved.

We were able to to successfully generate our benign model using the talc (instead of the proposed carbon nanotubes) as shown in Figure 1.

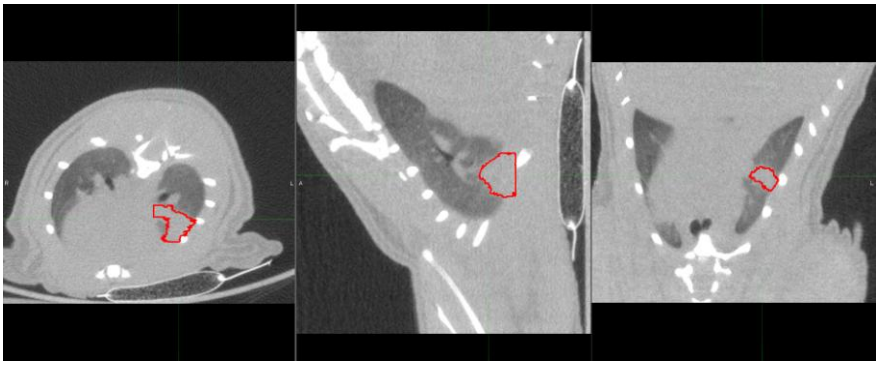

Figure 1: Axial, sagittal and coronal CT images of a benign nodule (talc), delineated in red in the left lung of a rat.

As soon as the capability of acquiring 4DCT images is restored on the GE-MicroCT scanner, we are ready to acquire and analyze the mechanical properties of the tumors and the benign tissue in accordance with the proposed method.

Specific Aim 3: Validate our method in a retrospective review of over 200 4D CT scans from patients previously treated in our department. *(**Dr. Loo**, Task 5 months 1 – 20)*

Task 5. Analyze approximately 200 4D CT images from previously treated patients and patients recruited within the funding period.

*5a. De-archive all previously acquired thoracic 4D CT scans and identify suitable patients for the study. Our institutional data (all 4D CT scans) are currently stored on DVD's. Data will be de-archived and suitable lung cancer patients (patients with benign and malignant pulmonary nodules) will be identified. (**Dr. Loo**, months 1 – 3)*

*5b. Identify benign and malignant pulmonary nodules to be included in the analysis and delineate nodules at each respiratory phase. (**Dr. Loo**, month 4)*

*5c. Perform simplified analysis by calculating the ratio of the volumes with respect to peak-inhale. (**Dr. Loo**, months 5-8)*

*5d. Analyze all 4D CT images and derive elasticity parameter by analyzing the displacement vector fields and perform statistical analysis (**Dr. Loo**, months 9-15)*

*5e. Analyze data from new patients acquired during the award period (**Dr. Loo**, months 15-18).*

*5f. Publish human study results (**Dr. Loo**, months 19-20)*

Status (Task 5): We continue to de-archive and analyze more patients. We have identified several patients with benign nodules (in addition to malignant nodules that were treated in our department). From those patients with benign nodules, 30% showed strong motion artifacts in 4DCT that aggravated the analysis. 23% of thus far analyzed patients have very small benign nodules. With the acquired CT resolution, the nodules are comprised of a few voxels. Deformable image registration for objects with such few voxels is inaccurate and 'noisy', thus the data will have limited value. Dr. Loo has started with the delineation of the benign and malignant nodules. Data will be processed and analyzed shortly.

Key Research Accomplishments:

Our first aim was to develop and validate an automated software package for determining PN elasticity against a manual contouring method, and preliminarily assess its ability to distinguish malignant tissue by comparing the elasticities of malignant PN with those of the lung. This work is now completed and a manuscript detailing the methodology and the results was submitted to 'Radiotherapy and Onclogy' (and included to this report).

Reportable Outcomes:

The following abstracts have been selected for POSTER presentation:

1. Mohammadreza Negahdar, Billy W Loo, Maximilian Diehn, Lu Tian, Dominik Fleischmann, and Peter G Maxim, *"Automated Tool for Determining Pulmonary Nodule Elasticity to Distinguish Malignant Nodules,"* ASTRO 2014

A manuscript summarizing our initial validation was submitted to Radiotherpay and Oncology. The abstract is included in the 'Supporting Documentation' section.

Conclusion:

We have successfully accomplished specific aim 1 of the proposed study. We now have a functional software to process and analyze 4DCT images to distinguish malignant and benign PN. Despite setbacks in time because of upgrades of the small animal equipment ad some difficulties with the human data, we believe we are on track to carry out the proposed research project.

Supporting Data:

Abstract submitted to the Annual Conference of ASTRO (2014):

Automated Tool for Determining Pulmonary Nodule Elasticity to Distinguish Malignant Nodules

Purpose: To develop and validate an automated method of determining pulmonary nodule (PN) elasticity against a manual contouring method, and preliminarily assess its ability to distinguish malignant tissue by comparing the elasticities of malignant PNs treated with stereotactic ablative radiotherapy (SABR) with those of the lung.

Methods: We analyzed breath-hold images of 30 patients with malignant PNs who underwent SABR in our department. A parametric nonrigid transformation model based on multi-level B-spline guided by Sum of Squared Differences similarity metric was applied on breath-hold images to determine the deformation map. The Jacobian of the calculated deformation map, which is directly related to the volume changes between the two respiratory phases, was calculated. Next, elasticity parameter will be derived by calculating the ratio of the Jacobian of the PN to the Jacobian of a 1cm region of lung tissue surrounding the tumor (E-ROI) as well as the Jacobian of the whole lung (E-Lung).

Results: For the first group of 15 patients we evaluated the volumetric changes of PNs and the lung from the maximum exhale phase to the maximum inhale phase, whereas the reverse was done for the second group of 15 patients. For the first group, mean and standard deviation for E-ROI and E-Lung were 0.91±0.09 and 0.86±0.18, respectively, which was verified by the manual method. For the second group, E-ROI and E-Lung were 1.34±0.27 and 1.57±0.51, respectively. These results demonstrate that the elasticity of the PNs was less than that of the surrounding lung ($p<0.0037$).

Conclusion: We developed an automated tool to determine the elasticity of PNs based on deformable image registration of breath-hold images. The tool was validated against manual contouring. Preliminarily, PN elastometry distinguishes proven malignant PNs from normal tissue of lung, suggesting its potential utility as a non-invasive diagnostic tool to differentiate malignant from benign PN.

Noninvasive Pulmonary Nodule Elastometry by CT and Deformable Image Registration

Mohammadreza Negahdar, Ph.D.,[*] Carolina E. Fasola, M.D., MPH,[*] Amy S Yu, Ph.D.,[*] Rie von Eyben, M.S.,[*] Tokihiro Yamamoto, Ph.D.,[§] Maximilian Diehn, M.D., Ph.D.,[*] Dominik Fleischmann, M.D.,[†] Lu Tian, Sc.D.,[‡] Billy W. Loo, Jr., M.D., Ph.D.,[*] Peter G. Maxim, Ph.D.[*]

Departments of [*]Radiation Oncology, [†]Radiology, and [‡]Health Research and Policy, Stanford University, Stanford, CA; [§]Department of Radiation Oncology, University of California, Davis, CA

Corresponding author:

Peter G. Maxim, Ph.D., Stanford Cancer Center, 875 Blake Wilbur Dr., Stanford, CA 94305. Tel: (650) 724-3018; Fax: (650) 725-8231; E-mail: pmaxim@stanford.edu

Billy W. Loo, Jr., M.D., Ph.D., Stanford Cancer Center, 875 Blake Wilbur Dr., Stanford, CA 94305. Tel: (650) 726-7143; Fax: (650) 725-8231; E-mail: bwloo@stanford.edu

Running title: CT Pulmonary Nodule Elastometry

Acknowledgement: This study has been supported by Department of Defense LCRP 2011 #W81XWH-12-1-0286.

Conflict of interest: None.

This paper has 14 pages, 5 figures, and 1 table. There is one more table as supplementary data.

Keywords: Malignant Pulmonary Nodule (MPN), Elasticity, Deformable image registration (DIR), X-ray CT, Lung Cancer.

Background and Purpose: To develop a noninvasive method for determining malignant pulmonary nodule (MPN) elasticity, validate it against manual contouring, and assess its ability to distinguish MPN from normal lung.

Methods and Materials: We analyzed breath-hold images at extreme tidal volumes of 23 patients with 30 MPN treated with stereotactic ablative radiotherapy. Deformable image registration (DIR) was applied to the breath-hold images to determine the volumes of the MPNs and a ring of surrounding lung tissue (ring) in each state. MPNs were also manually delineated on deep inhale and exhale images by two observers. Volumes were compared between observers and DIR by dice similarity. Elasticity was defined as the ratio of the volume change of MPN compared to ring.

Results: For all 30 tumors the dice coefficient was 0.79±0.07 and 0.79±0.06 between DIR with observers 1 and 2, respectively, close to the inter-observer dice value, 0.81±0.1. The elasticity of MPNs was 1.24±0.26, demonstrating that volume change of the MPN was less than that of the surrounding lung.

Conclusion: We developed a semi-automated CT elastometry method based on DIR that distinguishes biopsy-proven MPN from normal lung. Our data suggests that CT elastometry may be useful in distinguishing malignant from benign nodules.

Introduction

Elastometry provides tissue characterization that may help distinguish malignant from benign tissues, in contrast to static morphological imaging, which cannot provide this degree of information [1]. Several modalities of elasticity imaging, mostly based on ultrasound have been proposed and applied to a number of clinical applications including breast carcinoma [2,3], metastatic melanoma [4,5], head and neck carcinoma [6], and colorectal carcinoma [2]. However, since air is opaque in ultrasound images, this imaging modality has been considered insufficient for adequately visualizing lung tissue. Dynamic CT (including cine-CT and four dimensional (4D) CT) images the lung in different states of expansion that could be used to derive elasticity information in contrast to static three dimensional (3D) CT. In this study, we propose to develop pulmonary nodule elastometry derived from CT images acquired at breath-hold at extreme tidal volumes.

To demonstrate proof of principle that pulmonary nodule elastometry can be determined from breath-hold CT images at extreme tidal volumes, we analyzed the CT images of 23 patients with malignant pulmonary nodules (MPN) previously treated with stereotactic ablative radiotherapy (SABR) at our institution and compared the volume change of the treated MPN with that of the surrounding lung.

Methods and Materials

Patient Selection

From all patients treated on an institutional protocol of stereotactic ablative radiotherapy (SABR) for lung tumors between November 2011 and October 2012, 23 patients had both inhale and exhale breath-hold CT scans performed at the time of simulation available for review and are included in this analysis.

CT Imaging

Deep inspiration and natural expiration breath-hold CT scans for these patients were acquired on a Discovery ST PET/CT Scanner (General Electric Medical Systems, Waukesha, WI), using the following acquisition settings: 120

KVp, 110-195 mAs, 1.25 mm slice thickness, 0.97-1.36 mm pixel size, 500-700 mm display field of view. Images were reconstructed using either the built-in Bone Plus or Soft convolution kernel.

Contouring

The original treatment plans were delineated on either exhale or deep inhale and the clinically used contours were taken as reference. Two observers manually delineated the MPN on the opposite respiratory phase using our treatment planning software (Eclipse V11, Varian Medical Systems, Inc., Palo Alto, CA). To address inter-observer variability, the MPNs delineated by the two observers were compared to each other by calculating the dice similarity coefficient voxel-wise [7,8].

Deformable Image Registration

An intensity-based free-form deformable image registration (DIR) workflow was developed in MIM Maestro (MIM Software Inc., OH) and applied on extreme tidal volumes to determine the deformation map between deep inhale and natural exhale images. The underlying algorithm parameters were inherent in the program. The similarity and smoothness criteria were combined into one energy function, which was minimized in the registration process [9]. Since the main effect of respiration on MPN is the transition of MPN whereas deformation and volume change of MPN is minimal [10], we separate effect of large displacement between two extreme breath-hold images from volume changes of MPN itself. Therefore workflow starts with a tumor to tumor rigid registration with manual adjustment, followed by the DIR method which deforms the inhale image to exhale. Rigid registration and manual adjustment yield the advantage of robustness to the MPN location.

DIR Validation

We adopted dice similarity coefficient to assess the quality of overlap between the manually delineated contour and deformed contour [11]. As shown in **Figure 1 (a)**, for patients with MPNs originally delineated on inhale, DIR was

used to create an exhale contour. The deformed contour was then compared to the two manually delineated exhale contours using the dice similarity metric. Similarly and as shown in **Figure 1 (b)**, for patients with MPNs originally delineated on exhale, the two observers manually delineated contours on deep inhale. Next, DIR was used to create exhale contours from the manually delineated contours on deep inhale. These deformed contours were then compared to the clinically delineated contour by dice.

Quantitative Analysis of the Deformation Map

Because of the need for one-to-one correspondence between material points during continuous deformation, the calculated Jacobian determinant is required to be non-zero [12,13]. The degree of regional lung expansion is measured using the Jacobian determinant of the deformation map which is directly related to specific volume change [12].

$$J_n = \frac{V_n + \Delta V_n}{V_n} \tag{1}$$

where V_n is the volume of voxel element n, and ΔV_n is its change in a different respiratory cycle. A value of one implies no volumetric changes, while a Jacobian determinant greater than one, or smaller than one implies local tissue expansion or local tissue contraction, respectively. It therefore follows that for a continuous deformation to be physically possible, the Jacobian determinant must be greater than zero. We took advantage of this fact to evaluate the accuracy of the calculated deformation map.

To validate the volumetric changes as determined by the DIR method, we used the manually delineated MPNs. The volumetric changes were expressed as the ratio of the volumes in both phases.

$$\varphi = \frac{V_{exhale}^{MPN}}{V_{inhale}^{MPN}} \tag{2}$$

where φ is the manually measured of volume ratio of MPN, V_{inhale}^{MPN} is the volume of the MPN at deep inhale and V_{exhale}^{MPN} is the volume of the MPN at natural exhale.

Elasticity

We derived an elasticity parameter defined as the ratio of the volumetric change of the MPN to the volumetric change of a 1 cm ring of lung tissue surrounding the MPN, **Figure 2**:

$$d_\varepsilon = \frac{|J_{MPN}-1|}{|J_{Ring}-1|} \quad (3)$$

where J_{MPN} is the calculated volumetric ratio (exhale/inhale) of MPN and J_{Ring} is the calculated volumetric ratio (exhale/inhale) of a 1cm ring around the MPN. The normalization to the 1cm ring around the MPN, was introduced to remove the effect of MPN location and amount of motion in the lung, as both the MPN and the 1cm ring surrounding lung tissue undergo the same force. Based on the size of tumors, choosing 1 cm ring helps get fairly equal contribution of lung tissue and MPN into the calculated elasticity parameter. The calculated elasticity bigger than one ($d_\varepsilon > 1$) shows that the volume changes of MPN is more than that of the ring and the calculated elasticity smaller than one ($d_\varepsilon < 1$) shows that the volume changes of MPN is less than that of the ring.

Statistical Analysis

An equivalence test was performed to assess that the manually measured volume ratio was equivalent to the DIR calculated volume ratio of MPN. A paired t test was performed to compare the volume change of the normal tissue and the tumor tissue with both tissue samples coming from the same patient. All analyses were performed using SAS version 9.4 (SAS Institute Inc., Cary, NC, USA).

Results

Patient and Tumor Characteristics

We have included 23 lung cancer patients with non-small cell lung cancer (NSCLC) that were treated at our institution. The patient and tumor characteristics are given in **Table 1**.

DIR Validation

For all patients, the dice similarity coefficient between the delineated tumor by observer 1 and that of observer 2 is 0.81±0.1, whereas the dice value is 0.79±0.07 and 0.79±0.06 between DIR and observer 1 and DIR and observer 2, respectively. **Figure 3** shows an example of both delineated and deformed contours for a representative patient as well as the distribution of the calculated dice similarity for all patients. For all patients we calculated the Jacobian determinant of deformation map and validated the calculated volume ratio of MPN from the deep inhale phase to the natural exhale phase against the manual contouring. The calculated Jacobian determinant of deformation map within the lung is always greater than zero. We performed an equivalence test with the indifference zone defined as [-0.25, 0.25]. The mean of the differences of the paired values was 0.0293 with a 95% confidence interval of [-0.0176, 0.0761]. The 95% confidence interval falls completely within the indifference zone thus proving equivalence ($p<0.0001$). The average difference between the manually measured volume ratio of MPN (φ) and calculated volume ratio value via DIR was 0.02±0.15. **Figure 4** shows the calculated volume ratio by DIR versus manually measured volume ratio of MPN for all patients as well as the distribution of the difference between the calculated volume ratio and manually measured volume ratio of MPN for all patients which mainly concentrated around zero.

MPN Elasticity

For all patients of our study, the mean and standard deviation of the calculated volume ratio of the MPN and that of the 1cm ring surrounding lung tissue was 0.91±0.18 and 0.75±0.13, respectively. The mean and standard deviation of the difference between the calculated volume ratio of the MPN with that of 1 cm ring surrounding lung tissue was 0.16±0.15 ($p<0.0001$). **Figure 5 (a)** shows the calculated volume ratio of MPN and 1cm ring surrounding lung tissue for all patients. It mainly distributed below the unity line demonstrating that the volume ratio of the MPNs are less than that of the 1 cm ring surrounding lung tissue.

Finally, based on our definition of the elasticity parameter in Eq. 3, the mean and standard deviation of the calculated elasticity (d_ε) of the MPN was 0.78±1.1. **Figure 5 (b)** shows the distribution of the calculated elasticity for all patients.

Table 2 (supplementary data) shows tumor size in inhale and exhale as well as the calculated volume ratio of MPN by DIR and the calculated elasticity.

Discussion

We have designed and developed a method to determine the elasticity of MPNs based on deformable image registration of breath-hold CT images. Various deformable image registration methods [10,14-16] and mechanical indices [17] have been surveyed to calculate the most accurate and robust deformation map as well as differentiation metric, respectively. We developed a workflow that processed breath-hold images at extreme tidal volumes and calculated the volume change and the elasticity of MPNs.

We have demonstrated robust performance of the DIR method such that the difference between DIR and each of the observers is comparable to the inter-observer difference as assessed by Dice similarity. Our method can measure the volume ratio of MPNs, which can be either expansion or contraction. The accuracy of this measurement is demonstrated by the small difference between the manually measured volume ratios to that of the DIR method (0.02±0.15).

Based on the presented results in Figure 5 (a), $0 < J_{Ring} < J_{MPN} < 1$ which demonstrates that MPNs have a lesser volume change than the 1 cm ring surrounding lung tissue during exhalation. Thus, one expects $d_\varepsilon = \frac{|J_{MPN}-1|}{|J_{Ring}-1|} < 1$ which has been shown in Figure 5 (b), $(d_\varepsilon = 0.78 \pm 1.1)$. This demonstrated that MPNs have different characteristics in terms of elasticity compared to the surrounding lung tissue during respiration.

Different parts of the lung have different motion amplitudes and volume changes, which makes the calculated volume ratio of MPNs location-dependent. However the formulated elasticity is not location-dependent because the normalization of the volume change of MPN to that of the 1 cm ring surrounding lung tissue should remove the effect of MPN location, as both the MPN and the 1cm ring surrounding lung tissue undergo the same force, irrespective of their location. Therefore, it allows us to compare the elasticity of two different MPNs in two different locations of lung.

Our study does have certain limitations. First, our method was applied to a small number of patients, and focused only on proven MPNs, excluding benign nodules. The imaging protocol for all patients was not completely uniform

which resulted in different image resolutions that can impact the analysis. However we employed image interpolation so that DIR was applied to images of the same resolution.

To the best of our knowledge, this is the first study to calculate the elasticity of MPN from dynamic thoracic images. This provides the technical framework for testing the hypothesis that MPN and benign pulmonary nodule differ in elasticity. This difference may come from increased interstitial fluid pressure in tumors which can change the elasticity of MPN prior to any changes in morphological features. Studies have shown that most solid tumors have increased interstitial fluid pressure. This has been shown for breast carcinoma [2,3], metastatic melanoma [4,5], head and neck carcinoma [6], and colorectal carcinoma [2], with values as high as 60 mmHg. The tumor interstitial fluid pressure is uniform throughout the center of the tumor and drops steeply in its periphery.[18-20]. The mechanisms that determine the increased tumor interstitial fluid pressure are not fully understood, but are thought to involve blood-vessel leakiness, lymphatic vessel abnormalities, interstitial fibrosis and a contraction of the interstitial space mediated by stromal fibroblasts, all of which are hallmarks of cancer [21,22].

Since a limitation of current CT based screening for lung cancer is distinguishing malignant from benign nodule [23], our method could impact clinical practice by increasing the specificity of CT-based lung cancer screening. In addition CT elastometry may predict tumor aggressiveness that could potentially be used in multifocal lung cancer patients to ascertain and treat the most aggressive lesions first. Ultimately it may even be helpful to distinguish aggressiveness of different tumor regions to guide radiation therapy dose painting or adaptive boost design.

Future directions include applying our analysis to both proven malignant and benign nodules, and ultimately may differentiate the aggressiveness of tumors or tumor regions to aid radiation therapy target selection or dose painting. Strain tensor map along with elasticity can measure pulmonary nodule homogeneity in order to compare benign and malignant nodules. In addition we will attempt to extend our method to 4D CT images routinely acquired for radiotherapy simulation.

References

1. Sayyouh M, Vummidi DR, Kazerooni EA. Evaluation and management of pulmonary nodules: state-of-the-art and future perspectives. Expert opinion on medical diagnostics 2013;7:629-44.

2. Less JR, Posner MC, Boucher Y, Borochovitz D, Wolmark N, Jain RK. Interstitial hypertension in human breast and colorectal tumors. Cancer Research 1992;52:6371-4.

3. Nathanson SD, Nelson L. Interstitial fluid pressure in breast cancer, benign breast conditions, and breast parenchyma. Ann Surg Oncol 1994;1:333-8.

4. Boucher Y, Kirkwood JM, Opacic D, Desantis M, Jain RK. Interstitial hypertension in superficial metastatic melanomas in humans. Cancer Research 1991;51:6691-4.

5. Curti BD, Urba WJ, Alvord WG, et al. Interstitial pressure of subcutaneous nodules in melanoma and lymphoma patients: changes during treatment. Cancer Research 1993;53:2204-7.

6. Gutmann R, Leunig M, Feyh J, et al. Interstitial hypertension in head and neck tumors in patients: correlation with tumor size. Cancer Research 1992;52:1993-5.

7. Dice LR. Measures of the Amount of Ecologic Association Between Species. Ecology 1945;26:297-302.

8. Riegel AC, Chang JY, Vedam SS, Johnson V, Chi P-CM, Pan T. Cine Computed Tomography Without Respiratory Surrogate in Planning Stereotactic Radiotherapy for Non–Small-Cell Lung Cancer. International Journal of Radiation Oncology*Biology*Physics 2009;73:433-41.

9. Nie K, Chuang C, Kirby N, Braunstein S, Pouliot J. Site-specific deformable imaging registration algorithm selection using patient-based simulated deformations. Medical Physics 2013;40:-.

10. Wu J, Lei P, Shekhar R, Li H, Suntharalingam M, D'Souza WD. Do Tumors in the Lung Deform During Normal Respiration? An Image Registration Investigation. International Journal of Radiation Oncology*Biology*Physics 2009;75:268-75.

11. Liu X, Saboo RR, Pizer SM, Mageras GS. A shape-navigated image deformation model for 4D lung respiratory motion estimation. IEEE Int Symp Biomed Imaging; 2009. p. 875-8.

12. Reinhardt JM, Ding K, Cao K, Christensen GE, Hoffman EA, Bodas SV. Registration-based estimates of local lung tissue expansion compared to xenon-CT measures of specific ventilation. Medical Image Analysis 2008;12:752-63.

13. Negahdar M, Amini AA. Regional lung strains via a volumetric mass conserving optical flow model. IEEE International Symposium on Biomedical Imaging (ISBI): From Nano to Macro; 2012 May 2 - 5; Barcelona, Spain.

14. Negahdar M, Amini AA. Tracking planar lung motion in 4D CT with optical flow: validations and comparison of global, local, and local-global methods. In: Robert CM, John BW, editors. Medical Imaging 2010: Biomedical Applications in Molecular, Structural, and Functional Imaging; 2010 Sunday 14 February 2010; San Diego, CA, USA SPIE.

15. Chaojie Z, Xiuying W, Jinhu C, Yong Y, Dagan F. Deformable registration model with local rigidity preservation for radiation therapy of lung tumor. Image Processing (ICIP), 2012 19th IEEE International Conference on; 2012 Sept. 30 2012-Oct. 3 2012. p. 1673-6.

16. van Dam IE, van Sörnsen de Koste JR, Hanna GG, Muirhead R, Slotman BJ, Senan S. Improving target delineation on 4-dimensional CT scans in stage I NSCLC using a deformable registration tool. Radiotherapy and Oncology 2010;96:67-72.

17. Negahdar M, Dunlap N, Zacarias A, Eivelek AC, Woo SY, Amini AA. Strain as a novel index of regional pulmonary function from thoracic 4D CT images: in-vivo validation with tomographic SPECT ventilation and perfusion. Medical Imaging 2013: Biomedical Applications in Molecular, Structural, and Functional Imaging; 2013; Orlando, FA, USA SPIE.

18. Boucher Y, Baxter LT, Jain RK. Interstitial pressure gradients in tissue-isolated and subcutaneous tumors: implications for therapy. Cancer Research 1990;50:4478-84.

19. DiResta GR, Lee J, Larson SM, Arbit E. Characterization of neuroblastoma xenograft in rat flank. I. Growth, interstitial fluid pressure, and interstitial fluid velocity distribution profiles. Microvasc Research 1993;46:158-77.

20. Eikenes L, Bruland ØS, Brekken C, Davies CdL. Collagenase increases the transcapillary gradient and improves the uptake and distribution of monoclonal antibodies in human osteosarcoma xenografts. Cancer Research 2004;64:4768–73.

21. Heldin CH, Rubin K, Pietras K, Ostman A. High interstitial fluid pressure - an obstacle in cancer therapy. Nat Rev Cancer 2004;4:806-13.

22. Sarntinoranont M, Rooney F, Ferrari M. Interstitial stress and fluid pressure within a growing tumor. Ann Biomed Eng 2003;31:327-35.

23. Aberle DR, Adams AM, Berg CD, et al. Reduced lung-cancer mortality with low-dose computed tomographic screening. N Engl J Med 2011;365:395-409.

Table 1. Patient and tumor characteristics.

Characteristic	Value (%)
All Patients	*23*
Gender	
Male	*13 (57)*
Female	*10 (43)*
Age, y	
Median	*66*
Range	*35-94*
Tumors	30
Primary/Secondary	*18/12*
Radius of Tumors, cm (treatment planning)	
Mean	*1.06*
Range	*0.3-2.1*
Volume of Tumors, cm^3 (treatment planning)	
Mean	*4.9*
Range	*0.11-38.8*
Volume of Tumors in opposite phases, cm^3 (Obs 1)	
Mean	*7.6*
Range	*0.13-39.62*
Volume of Tumors in opposite phases, cm^3 (Obs 2)	
Mean	*7.58*
Range	*0.13-39.74*

Table 2. Raw data of all tumors from inhale to exhale for current study. Second and third columns show the average of manually delineated MPN by two observers in inhale and exhale, respectively. Fourth column shows the calculated volume ratio of MPN by DIR. Fifth column shows the calculated elasticity of MPN by Equation (3).

Tumor	Tumor Size (cm^3) (Inhale) Manual	Tumor Size (cm^3) (Exhale) Manual	Calculated volume ratio of the MPN DIR	Elasticity (d_ϵ) Equation (3)
1	17.48	17.19	0.96	0.22
2	12.08	12.07	1.15	1.35
3	0.139	0.125	0.68	0.87
4	0.997	1	0.52	1.42
5	1.74	1.7	0.98	0.14
6	3.75	3.85	1.08	1.55
7	8.61	8.57	1.00	0.01
8	7.03	7.54	1.16	0.75
9	22.62	24.4	1.03	0.08
10	11.46	11.23	1.02	0.06
11	7.18	7.06	0.90	0.43
12	9.63	9.77	1.00	0.04
13	3.69	3.95	0.97	0.12
14	0.497	0.462	0.56	0.93
15	7.33	7.33	0.93	0.68
16	4.99	4.45	0.91	0.32
17	3.42	2.33	0.94	0.18
18	39.61	38.36	0.99	0.63
19	19.53	17.3	0.89	0.53
20	3.74	4.1	1.18	5.94
21	2.45	2.47	1.26	1.93

22	9.04	8.91	0.95	0.2
23	0.81	0.759	0.69	0.82
24	3.84	2.31	0.90	0.17
25	1.72	1.22	0.69	0.68
26	12.35	10.58	0.93	0.32
27	0.39	0.38	0.73	0.81
28	0.901	0.864	0.60	1.12
29	1.32	1.1	0.72	0.94
30	12.34	12.02	0.96	0.14

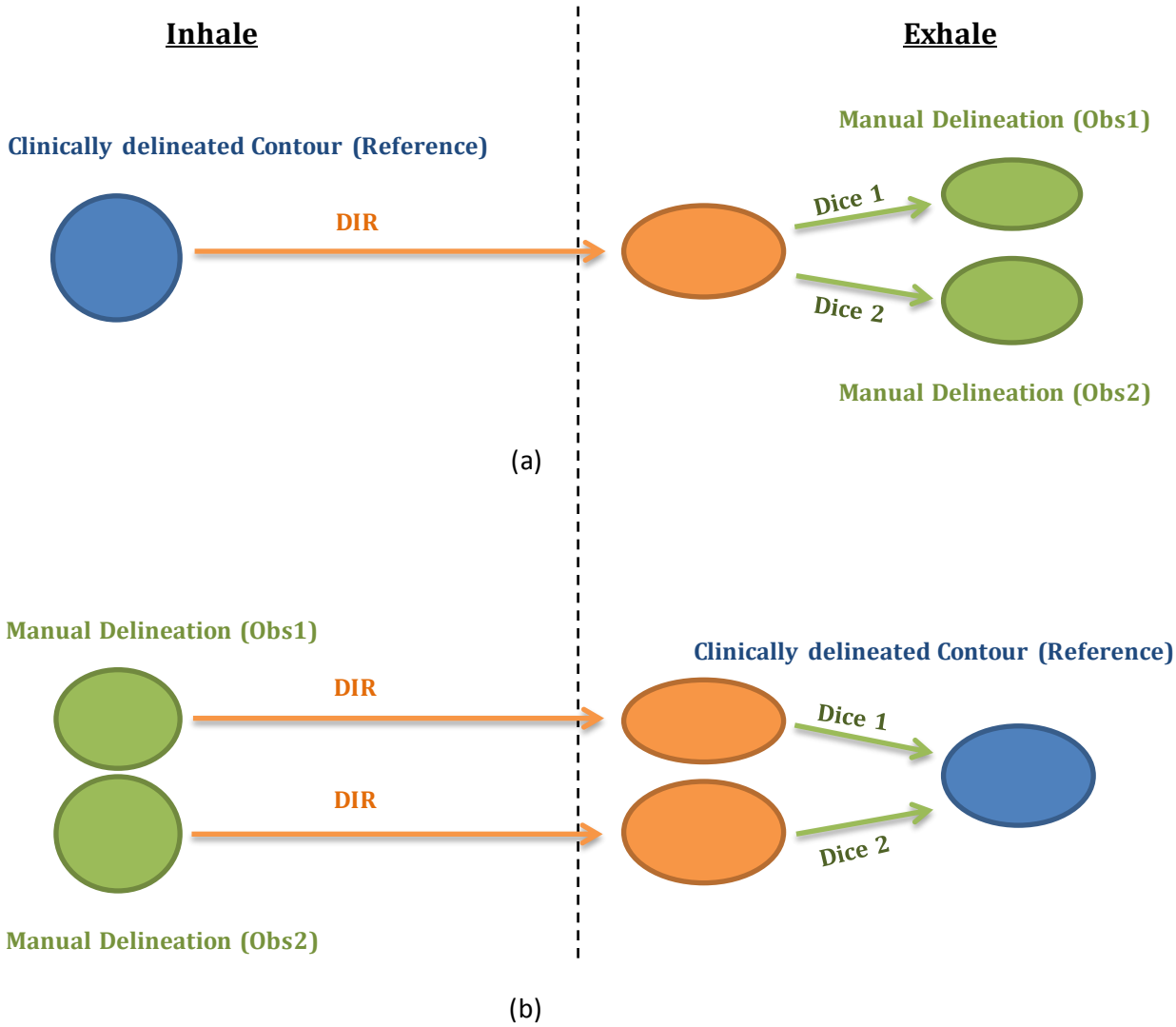

Figure 1. (a) Patients with MPNs originally delineated on inhale; DIR was used to create an exhale contour. The deformed contour was then compared to the two manually delineated exhale contours using the dice similarity metric and average of the dice values has been reported. (b) Patients with MPNs originally delineated on exhale; DIR was used to create two exhale contours from the manually delineated contours on inhale. Then the deformed contours were compared to the clinically delineated contour by dice and average of the dice values has been reported.

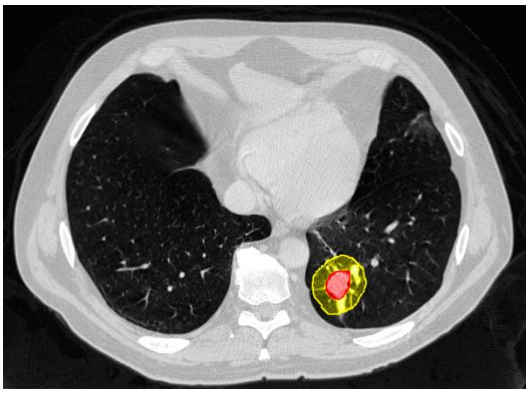

Deep Inhale CT

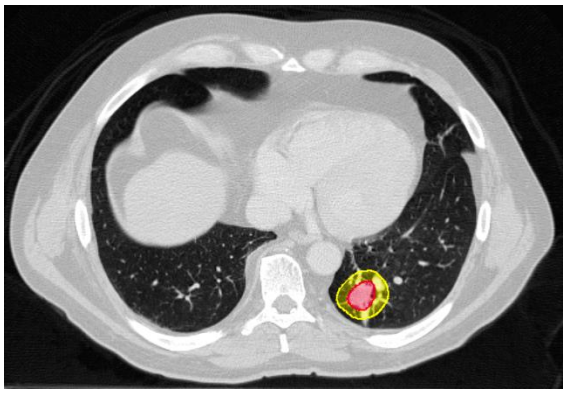

Natural Exhale CT with Deformed Contours

Figure 2. An axial view of a representative patient; delineated MPN (red) and 1cm ring of the surrounding lung (yellow) for deep inhale (left column) and deformed MPN and ring contours superimposed on exhale image (right column) for the purpose of elasticity calculation.

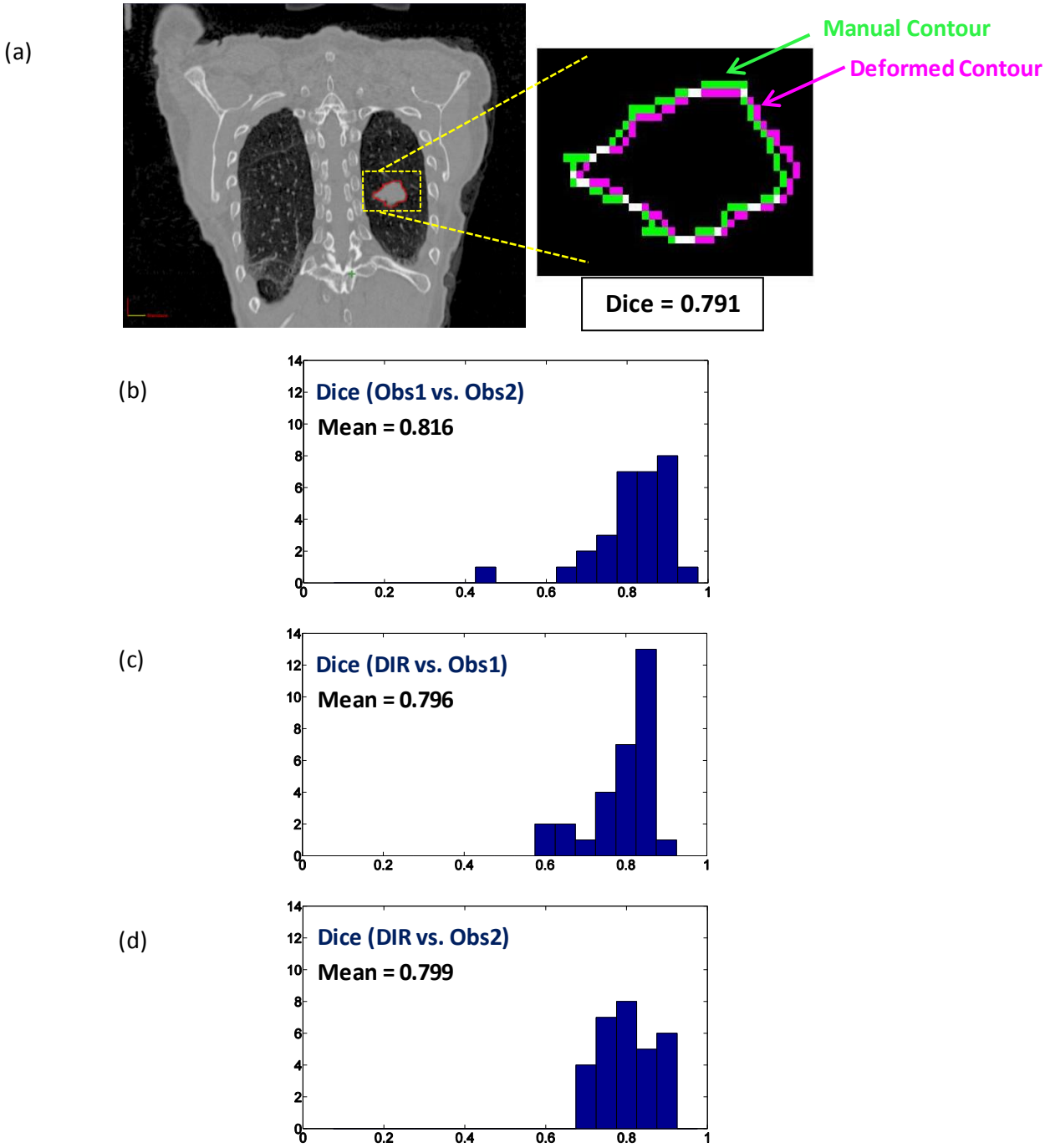

Figure 3. (a) A coronal view of a manually delineated tumor in exhale of a representative patient; delineated MPN in exhale (green) and delineated MPN in inhale deformed into the exhale (magenta), Dice similarity for this patient is 0.791. (b) Distribution of the calculated Dice similarity metric between the manually delineated MPN by first observer with that of second observer. (c) Distribution of Dice similarity between the delineated MPN in inhale deformed into the exhale phase by DIR with the manually delineated MPN by first observer in exhale. (d) Distribution of Dice similarity between the delineated MPN in inhale deformed into the exhale phase by DIR with the manually delineated MPN by second observer in exhale. Based on dice similarity, we conclude that DIR compares favorably to manual contouring within inter-observer differences.

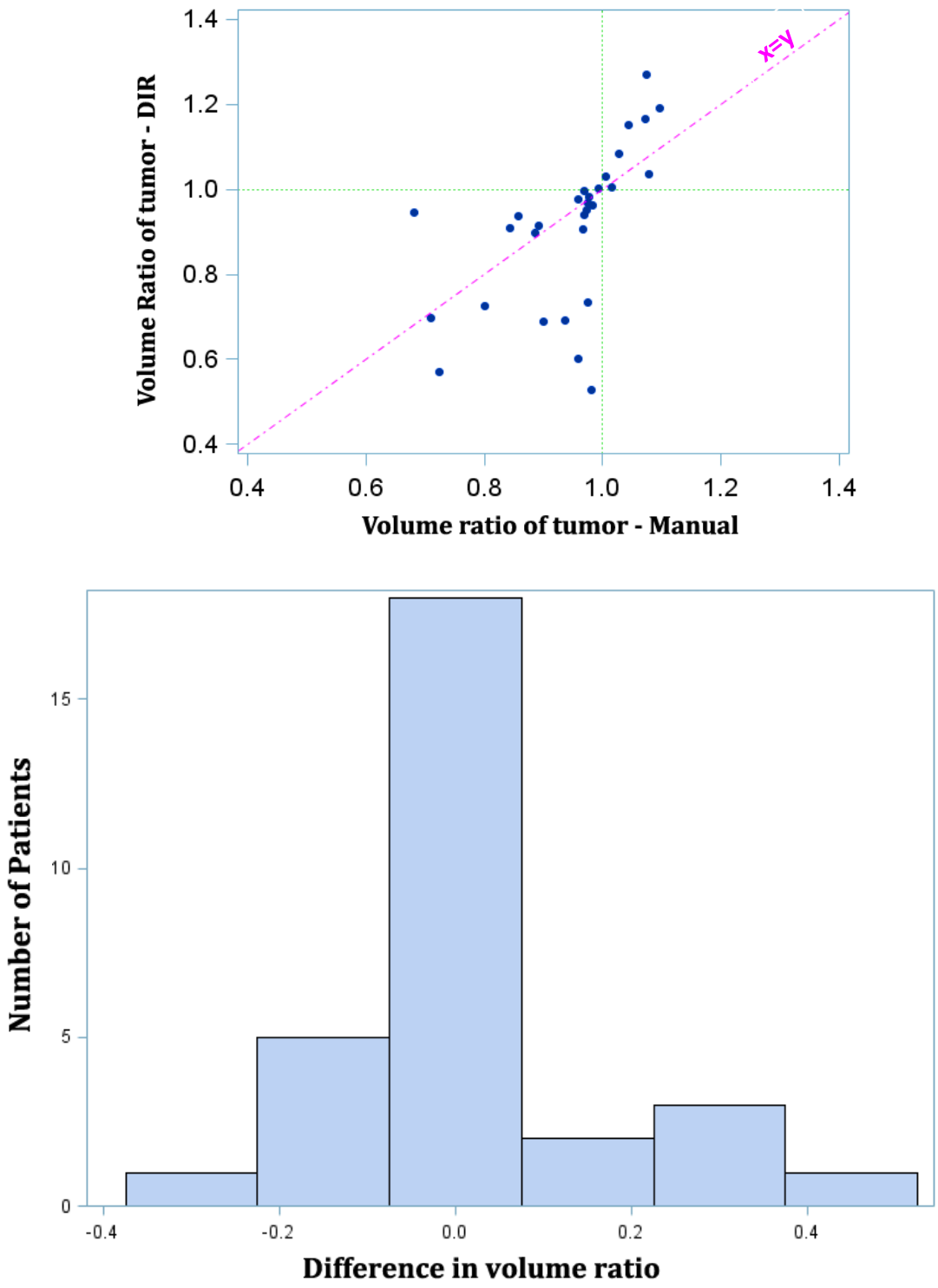

Figure 4. (Up) Calculated volume ratio of MPN versus manually measure of volume ratio of MPN (Equation (2)) for all 30 patients from inhale to exhale. Green dashed line shows unity Jacobian value equivalent to no volume changes. Red line represents the identity line. (Bottom) Distribution of the difference between the calculated volume ratio by DIR from inhale to exhale with manually measured volume ratio of MPN (0.02±0.15).

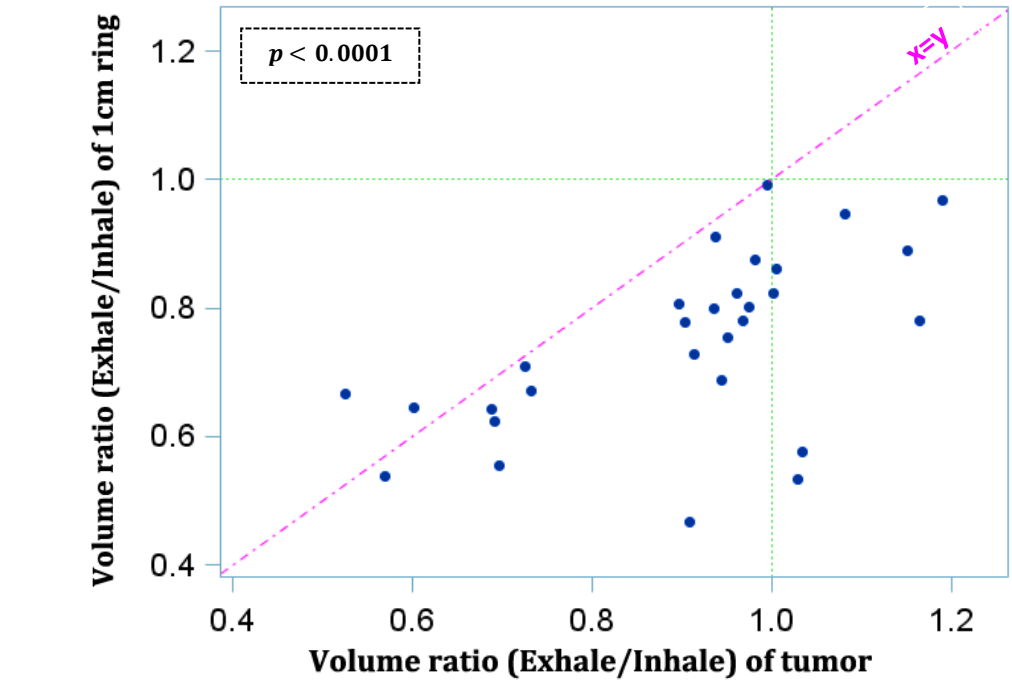

(a)

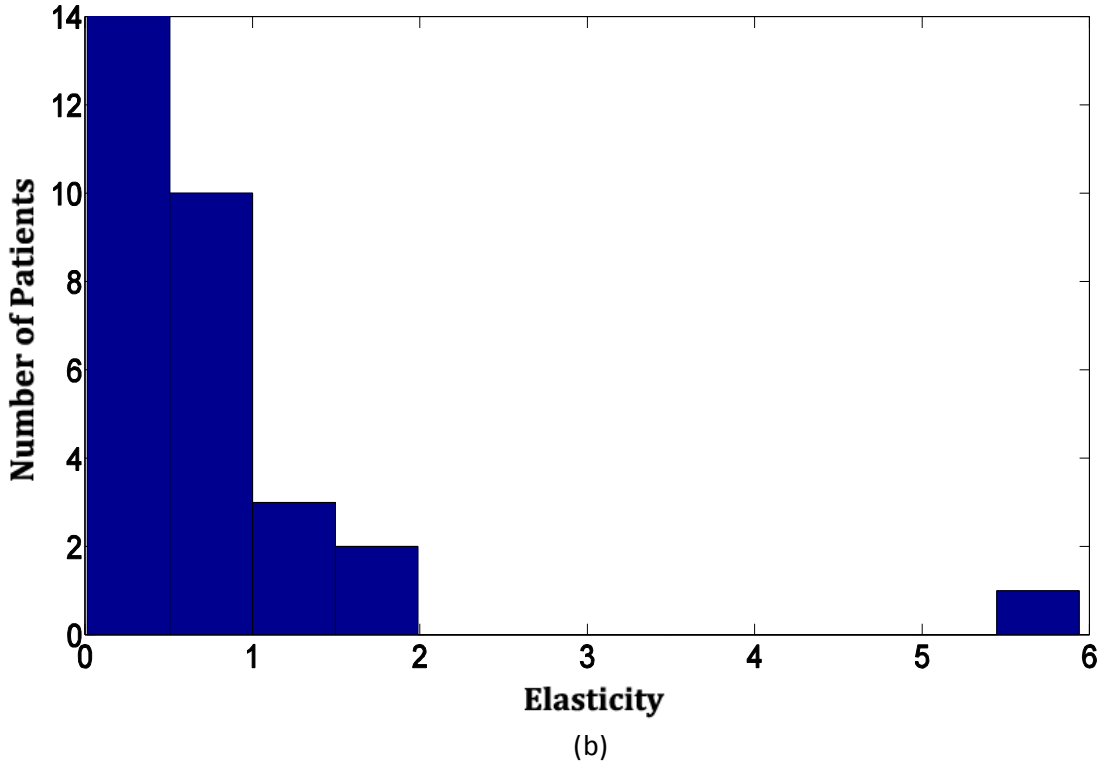

(b)

Figure 5. (a) Calculated volume ratio of 1 cm ring of surrounding lung (0.75±0.13) versus that of tumor (0.91±0.18) for all patients. Green dashed line shows unity Jacobian value equivalent to no volume changes. Red line represents the identity line. (b) Distribution of the calculated elasticity by Equation (3) from inhale to exhale (0.78±1.1).